JOURNAL OF GEOPHYSICAL RESEARCH, VOL. 114, A02301, doi:10.1029/2007JA012808, 2009

Role of the equatorial ionization anomaly in the development of the evening prereversal enhancement of the equatorial zonal electric field

S. Prakash,[1] D. Pallamraju,[1] and H. S. S. Sinha[1]

Received 7 September 2007; revised 22 October 2008; accepted 7 November 2008; published 4 February 2009.

[1] During the evening prereversal enhancement of the zonal electric field (EPRE) that begins around 1700 LT when the *F* region neutral winds turn eastward, as assumed here, and continues till the postsunset zonal electric field reversal time, an overall positive feedback is shown to occur between the eastward electric field in the lower side of the flux tube integrated (LSFTI) *F* region and the increased flux tube integrated Pedersen conductivity (FTIC) of the tropical *F* region. The increase in this FTIC can take place because of the increase in electron density through the increase in solar flux and the intensification of the equatorial ionization anomaly (EIA). While the influence of EIA on EPRE is immediate, the growth time for EIA is 2 to 3 h. Therefore, for a strong EPRE to occur, a fairly strong EIA is required at 1700 LT which is then sustained by the electric field associated with EPRE during its growth period. This study suggests that the postsunset eastward electric field is due to the combined currents in the equatorial electrojet and the LSFTI *F* regions that get diverted from the daytime Sq current system and flow from the presunset region toward the postsunset zonal electric field reversal region. Thereafter these currents turn and flow poleward to meet the current continuity requirement of the *F* region dynamo followed by a westward turn to rejoin the daytime Sq current system in midlatitudes. Thus the currents responsible for EPRE are an extension of the daytime Sq current system.

Citation: Prakash, S., D. Pallamraju, and H. S. S. Sinha (2009), Role of the equatorial ionization anomaly in the development of the evening prereversal enhancement of the equatorial zonal electric field, *J. Geophys. Res.*, *114*, A02301, doi:10.1029/2007JA012808.

1. Introduction

[2] Studies using the VHF backscatter radar at Jicamarca (12°S, 77°W; dip 2°N) and the HF Doppler radar at Trivandrum (8.5°N, 77°E; dip 0.5°N) have shown that on many days the daytime eastward electric field in both *E* and *F* regions enhances during late evening hours before its westward reversal at a later time [*Woodman*, 1970; *Balsley*, 1973; *Fejer et al.*, 1979; *Fejer*, 1981; *Jayachandran et al.*, 1987]. This enhancement in the eastward electric field, referred to as the EPRE, gives rise to enhancement in the vertical drift velocity of the *F* layer, which can be as large as 70 m s^{-1} [*Woodman*, 1970]. Statistically, an increase in the altitude of the *F* layer is positively correlated with the occurrence of the equatorial spread *F* (ESF) [*Farley et al.*, 1970]. Therefore, a good understanding of the EPRE is essential to gain knowledge of the evening equatorial upper atmospheric processes, including the ESF. Magnitude of the EPRE varies from night to night and is a function of various factors such as the season, level of geomagnetic activity, and the phase of the solar cycle.

[3] It is generally believed that the EPRE is linked to the *F* region dynamo. A number of numerical models of global and equatorial electric fields have been developed to explain the EPRE phenomenon [*Rishbeth*, 1971; *Heelis et al.*, 1974; *Stening*, 1981; *Takeda and Yamada*, 1987; *Crain et al.*, 1993; *Eccles*, 1998; *Du and Stening*, 1999; *Fesen et al.*, 2000]. *Farley et al.* [1986] proposed a mechanism wherein the enhanced electric field is developed during and after the sunset when both the Hall and the Pedersen conductivities in the off-equatorial *E* region decrease rapidly from their daytime values and the zonal winds in the *F* region are eastward. *Haerendel and Eccles* [1992] proposed that after sunset the zonal Cowling conductivity gradients in the equatorial electrojet (EEJ) in combination with the current continuity requirement (CCR) from the evening *F* region dynamo might have a causal relationship with the EPRE mechanism. Using a numerical simulation *Eccles* [1998] inferred that the EEJ could only be a limited modifier of the EPRE. On the basis of the preliminary study by *Rishbeth* [1971], *Eccles* [1998] showed that the enhanced zonal electric fields are due to the requirement of the rapidly changing vertical electric fields near the sunset to be curl-free.

[4] The present work is an attempt to demonstrate that the peak vertical drift (V_p) associated with the EPRE can undergo significant modification due to an increase in the FTIC of the tropical *F* region and thus accounting for the increase in the V_p with solar flux. In this mechanism, this change in the FTIC in *F* region and the invigoration of the equatorial *F* region fountain leads to a positive feedback between the EIA and the eastward electric field when the neutral winds are eastward.

[1]Physical Research Laboratory, Ahmedabad, India.

0148-0227/09/2007JA012808

[5] A strong link between the EPRE and the ESF is well established in the literature. Here, we propose a strong link between the EIA and the EPRE when the neutral winds are eastward. These studies together provide a theoretical/observational basis for the link between the EIA and the ESF. In fact, measurements by optical and radio techniques from the Indian longitudes [*Raghavarao et al.*, 1988; *Rastogi et al.*, 1989; *Sridharan et al.*, 1994] and the American longitudes [*Mendillo et al.*, 2001; *Valladares et al.*, 2001; *Pallamraju et al.*, 2004] do show a good correlation between the strength of the EIA and the occurrence of the ESF.

[6] This paper has been organized into the following sections: Section 2 describes the proposed mechanism, section 3 presents the derivation of equations used, section 4 describes the results of the numerical simulation of the zonal electric field during the low and high solar flux periods, and section 5 presents the discussion and summary of the present study.

2. Description of the Model for the EPRE

[7] Typical features of the eastward electric field associated with the EPRE as observed over Jicamarca [*Fejer et al.*, 1991] during equinoxes are (1) the eastward electric field increases monotonically between 1700 and 1900 LT and maximizes at around 1900 LT, denoted here by TF 1; (2) thereafter, it decreases and reverses westward at around 2000 LT, denoted here by TF 2; and (3) the peak value of the eastward electric field increases with the increase of solar flux denoted here by TF 3. The proposed mechanism explains all the above three typical features. An increased eastward neutral wind in the thermosphere and a rapid decrease in the FTIC of the *E* region during the postsunset period are factors that are mainly responsible for the development of the EPRE [*Rishbeth*, 1971; *Heelis et al.*, 1974]. We call these two factors as key factor 1 (KF1) and key factor 2 (KF2). The peak amplitude of V_p associated with the EPRE can increase by as large as a factor of three from the low to the high solar flux periods [*Fejer et al.*, 1991; *Namboothiri et al.*, 1988]. In this study we show that an increase in the FTIC in the *F* region due to the increase of solar flux results in an increase in the EPRE magnitude. We name this factor as the key factor 3 (KF3).

[8] It has been suggested [e.g., *Heelis et al.*, 1974; *Tsunoda*, 1985; *Batista et al.*, 1986; *Goel et al.*, 1990] that the longitudinal gradient of integrated Pedersen conductivity (LGIPC) in the *E* region at sunset time can play a positive role in strengthening the EPRE magnitudes. *Tsunoda* [1985] has shown that the occurrence maxima in scintillation activity at a given longitude are coincident with time of the year when the sunset is simultaneous at the conjugate *E* layer. For a given ratio of conductivity in the *E* region from day to night, LGIPC increases with decrease of sunset duration thus indicating that the scintillation activity at a given longitude increases with the increase of LGIPC. *Batista et al.* [1986] find that the relationship between the sunset duration that affects the LGIPC in the *E* region at sunset time and the V_p does not seem to be all that straightforward. For example, over Huancayo the amplitudes are greater during summer than during winter months, but the sunset duration in December are greater than in July, showing that there may be other factors, besides the LGIPC in the *E* region, that have influence on the V_p amplitudes. In addition to the zonal wind, we believe that the other factor could be the current flow paths which may, during a given season depend on declination angle and angle between the magnetic meridian and the solar terminator. The study of the seasonal variation of V_p is therefore not suitable for the determination of the exclusive influence of LGIPC in the *E* region on V_p. In connection with the variation of V_p with solar flux, *Goel et al.* [1990] using *E* region model by *Muggleton* [1975] found that because of the variation in electron density from low to high solar flux period, the LGIPC in the *E* region increases by a factor of two. They suggested that theoretical calculations of V_p incorporating the above variation in the LGIPC in the *E* region be made to assess the role of these gradients in explaining observed variations in V_p with increase of solar flux. A model study of electron density in the *E* region by *Johnson* [1961] also shows that the ratio of electron density in the *E* region from daytime to that in the nighttime increases by a factor of two from the low to the high solar flux period. From our model simulation we found that an increase in the LGIPC by a factor of two gives rise to an increase in the EPRE magnitude which is much smaller than a factor of three. The results of the study are described in section 4.4.

[9] The local time of occurrence of the peak of EPRE is around 1900 LT which coincides with the local time at which the conductivity in the *E* region acquires its nighttime value [*Haerendel and Eccles*, 1992]. Hence the TF 1 indicates the possibility of the EPRE being influenced by the flow of currents in the EEJ region from the presunset side. As the conductivity of the *E* region is not expected to vary appreciably after acquiring its nighttime value, the decrease in the electric field following its peak value can be accounted for only if these currents take a turn and flow upward/poleward. Such a current flow will also meet the CCR of the *F* region dynamo driven by the eastward zonal winds in the *F* region. The electric field reversal after this decrease in the electric field can be accounted for if westward currents flow into this region from the following morning side.

[10] In the proposed mechanism, the electric field is produced through a flow of current in the region where the EPRE is observed. From the generalized Ohm's law one can see that the current over a given path is a function of both neutral winds and conductivities and hence, the zonal electric field is dependent only on winds and conductivities in the *E* and *F* regions. During the postsunset period neutral winds in the *F* region dominate over those in the *E* region and hence for reasons discussed in section 3, we ignore the effects of the neutral winds in the *E* region. From low to high solar flux periods, model neutral winds in the *F* region increase on an average by less than 20% in the southern hemisphere [*Hedin et al.*, 1991]. This variation in neutral winds is too small to account for the large variation (by factor of three) observed in V_p from low to high solar flux periods. Therefore, we have examined whether the expected variation in the FTIC of the *F* region with the solar flux can account for the observed increase in the strength of the EPRE from low to high solar flux conditions. We also examined whether the increase in LGIPC in the *E* region due to the change of solar flux, as suggested by *Goel et al.* [1990], can account for the increase of the EPRE from the low to high solar flux period. For developing a mechanism to explain the TF 3 we limit our discussion exclusively to equinoxes for an equatorial station with zero declination angle. For such a location, during

equinoxes the solar terminator is parallel to the geomagnetic field lines and parameters such as the zonal and the meridional winds are symmetric with respect to the magnetic equator [*Abdu et al.*, 1981]. Seasonal variations add more complexity in both calculations and visualization of the proposed mechanism. However, we expect that with some modifications this mechanism would be applicable to other seasons as well.

[11] A morphological study of the total electron content (TEC) variation by *Jee et al.* [2004] showed that during high solar flux periods, TEC values at the crests of the anomaly (around ±15° Mag. Lat.) and in the regions poleward of the EIA crests (between ±15° and ±30° Mag. Lat.) are nearly three times larger when compared to those during the low solar flux periods. Numerical simulation by *Klobuchar et al.* [1991] shows that at around 2000 LT, the peak electron density N_{max} is about 4×10^6 cm^{-3} at 25° latitude and about 2.6×10^6 cm^{-3} at 30° latitude during solar maximum. On the other hand, during periods of solar minimum, even with a large zonal electric field/vertical drift, the N_{max} values at the same time and latitude are about 10^6 cm^{-3} and 6.0×10^5 cm^{-3}. It can, therefore, be seen that the electron density during periods of high solar flux is nearly four times larger than that during the periods of low solar flux. A model study by *Hanson and Bamgboye* [1984] showed that with the increase of solar flux from 75 to 200, the Pedersen conductivity per ion increased by a factor of about 3.0 (at 300 km) to about 5.6 (at 450 km). In view of the above, the conductivity in the *F* region and hence the FTIC in the *F* region can increase by a large factor from low to high solar flux periods. This is well represented by the model studies of the *F* region FTIC for the low and high solar flux periods [*Anderson et al.*, 1987]. The expressions for the zonal electric field as per section 3 require normalized *F* region FTIC values for the estimation of the zonal electric field. From *Haerendel and Eccles* [1992], the *E* region FTIC acquires nighttime value at 1900 LT and they are assumed to remain the same thereafter. The required values of the *F* region FTIC normalized to the *E* region FTIC conductivity at 2100 LT is given by *Anderson et al.* [1987, Figure 9]. Two main features of the normalized FTIC of the *F* region profiles are (1) the *F* region FTIC in the 200 km to 300 km region during low solar flux period are nearly the same as in the 350 to 450 km region during the high solar flux period and (2) when the base of the normalized FTIC profiles for the two periods are matched, the ratio of normalized FTIC of the two periods increases with altitude maximizing at 1100 km altitude. The average ratio of the normalized FTIC for the two periods was about four.

[12] *Prakash and Muralikrishna* [1981] found that during the postsunset period over Jicamarca, the zonal electric field in the equatorial *F* region remains in the same direction as in the EEJ. Also the zonal electric field in the equatorial *F* region is generally larger than that in the EEJ region indicating that the *F* region plays an important role in the development of the EPRE. Studies of *McClure and Peterson* [1972] and *Pingree and Fejer* [1987] show that during late evening hours the zonal electric field in the LSFTI *F* region (below 650 km) remains in the same direction as in the EEJ region. On the basis of the above, it is proposed that the currents from the presunset side flow in a parallel combination of the EEJ and the LSFTI *F* regions to meet the CCR of the *F* region dynamo.

[13] Model zonal neutral winds in the equatorial thermosphere reverse from the westward to the eastward direction at around 1700 LT [*Hedin et al.*, 1991]. Thereafter the magnitude of these eastward winds increases till 2030 LT followed by a monotonic decrease. The conductivity of the *F* region decreases slowly after sunset and therefore, after sunset the dynamo action due to these winds is expected to maximize at around 2030 LT resulting in a strong penetration of zonal currents from the presunset side into late evening hours. Further, currents not only from the presunset side but also from the following morning side contribute to the CCR of the *F* region dynamo. In the present mechanism, the dynamo action is by the zonal winds in the *F* region. The base of the *F* region is around 200 km and 350 km respectively, for low and high solar flux periods [*Anderson et al.*, 1987]. Therefore, we use 200 and 350 km as reference altitudes for the calculation of currents during the low and high solar flux periods. A schematic diagram of the proposed current flow path is shown in Figure 1. The *x* axis represents the local time (and also the longitudinal extent), while the *y* axis represents the altitude over the magnetic equator (but not to scale). The parameter z represents the latitudinal distance corresponding to a given latitude λ from the equator. The details of the shortest current path $(S_{CP})_z$ are given in sections 4.1 and 4.2. For the sake of clarity, $(S_{CP})_z$ is projected along the *y* axis and IM represents $(S_{CP})_z$ for a given geomagnetic latitude λ (or equivalent z) from the geomagnetic equator. The zonal electric field decreases with altitude and reverses from east to west at an altitude J. This altitude of the reversal region J is denoted as Z_{EFRR-2}. It is proposed that the dynamo action by the zonal winds and the electric fields discussed above would drive two current loops, one in the prezonal electric field reversal region 1, Z_{EFRR-1}, (shown as the current loop ABCDE) and the other during the post-Z_{EFRR-1} (shown as current loop PQRS). Z_{EFRR-1} is shown at the longitude corresponding to 2000 LT. In addition to these two current systems shown as ABCDE and PQRS there is a third one (not shown here), which is the westward Hall current that flows through Z_{EFRR-1}. This current is prevalent in the *E* region that is field line connected to the *F* region where the neutral winds in the *F* region are eastward. These neutral winds give rise to a downward/equatorward electric field that drive the westward Hall current in the field line connected *E* region as suggested by *Farley et al.* [1986].

[14] The current from the following morning side, that meets the CCR of the *F* region dynamo during the postsunset period, consists of the westward Pedersen current. This current is driven by the westward electric field produced because of the potential difference between the dusk and the following dawn terminators and, therefore, it can be assumed to be largely independent of the CCR of the *F* region dynamo during the postsunset period. If the current from the following morning side exceeds the CCR of the postsunset *F* region dynamo, then the excess current would flow westward pushing the Z_{EFRR-1} toward the dusk side. On the other hand if the above current is inadequate to meet the CCR of the *F* region dynamo, then negative charges would accumulate at the base of the *F* region (and positive charges higher above) giving rise to (1) an eastward electric field in the pre-Z_{EFRR-1} region and (2) an additional westward electric field in the post-Z_{EFRR-1} region. The longitudinal distance between the dusk terminator and the Z_{EFRR-1} is many times smaller than

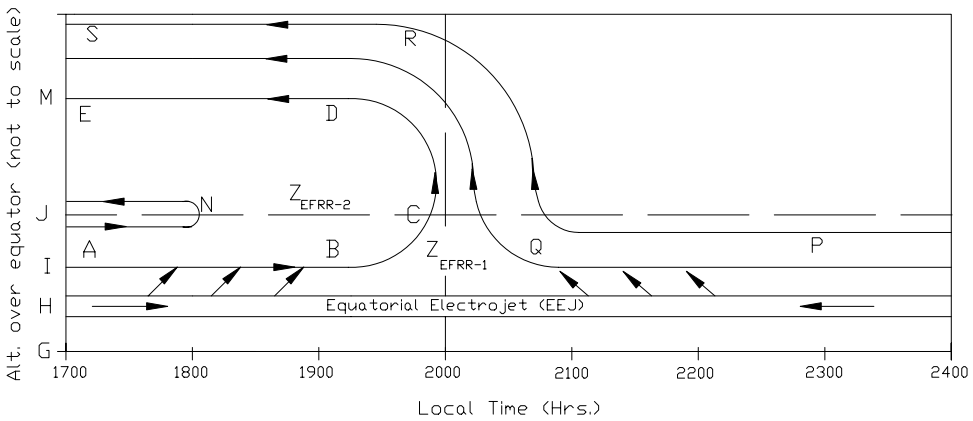

Figure 1. A sketch of the flow paths of the flux tube integrated currents is shown in the plane perpendicular to the geomagnetic field lines as projected on to the geomagnetic equatorial plane during the evening and postsunset period. The *x* axis represents the local time (and also the longitudinal extent), and the *y* axis represents vertical distance in kilometers on an arbitrary scale. The letter G represents the ground level, and H represents the EEJ altitude. I represent the altitude of the base of the *F* region which is at 200 km for case 1 and at 350 km for case 2. The geomagnetic latitudes defined in this study are with respect to the altitudes of 200 and 350 km. Thus, I also represents the geomagnetic equator in both the cases. J represents the altitude of equatorial zonal electric field reversal region, Z_{EFRR-2}. IM represents $(S_{CP})_z$ in kilometers corresponding to the geomagnetic latitude, λ_R, at which the currents rejoin the daytime Sq current system. It may be noted that below 650 km, the altitude of a field line and $(S_{CP})_z$ are nearly the same. ABCDE schematically represents the possible path of the current that flows from the presunset toward the postsunset zonal electric field reversal region (Z_{EFRR-1}). This current then turns upward to meet the current continuity requirement of the *F* region dynamo in the prezonal electric field reversal region. PQRS is the possible path of current that flows from the morning sector of the following day.

that between the Z_{EFRR-1} and the dawn terminator of the following day. As a result, the eastward electric field produced in the pre-Z_{EFRR-1} because of this charge deposition would be many times larger than the additional westward electric field produced in the post-Z_{EFRR-1}.

3. Expressions for Currents and Electric Fields

[15] In the thermosphere, magnetic field lines can be treated as equipotentials for electric field structures larger than a few kilometers [*Farley*, 1959]. As the scale sizes of the phenomena considered in the present study are in tens of kilometers, FTI variables have been used in the estimation of currents and electric fields. The integration model collapses the ionosphere into a two-dimensional geomagnetic equatorial plane. Here the FTI quantities are represented in a polar coordinate system (L, φ) placed in the equatorial plane where L is the McIlwain parameter geocentric distance measured in earth radii, R_E, and φ is the magnetic longitude in degrees. The local radii "r" on a geomagnetic field line expressed in units of R_E is described by:

$$r = L\left(\cos^2\lambda\right) \tag{1}$$

where λ is the magnetic latitude. A two-layer model has been used in this study wherein 150 km altitude is the dividing line between the *E* and the *F* regions. The currents and the electric fields are related to the neutral winds through the generalized Ohm's law. Additionally, they must satisfy the conditions of the current continuity ($\nabla \cdot J = 0$) and the curl free nature of the electric field ($\nabla \times E = 0$). Using the FTI variables and the above coordinate system, the currents J_φ and J_L can be written from the generalized Ohm's law as:

$$J_\varphi = \Sigma_{PE}\left(E_\varphi - BW_{LPE}\right) + \Sigma_{HE}\left(E_L + BW_{\varphi HE}\right) + \Sigma_{PF}\left(E_\varphi - BW_{LPF}\right) \tag{2}$$

$$J_L = \Sigma_{PE}\left(E_L + BW_{\varphi PE}\right) - \Sigma_{HE}\left(E_\varphi - BW_{LHE}\right) + \Sigma_{PF}\left(E_L + BW_{\varphi PF}\right) \tag{3}$$

where J_φ is the integration of the zonal current component and J_L is the integration of the transverse current component in the meridional plane. E_φ and E_L represent electric fields along the coordinates φ and L. Over a given geomagnetic field line, subscripts E and F denote variables in the *E* and *F* regions, and subscripts P and H denote variables that are a result of Pedersen and Hall conductivity weighted integration over the flux tubes. Σ_{PE}, Σ_{HE}, and Σ_{PF} represent the FTI Pedersen and Hall conductivities in the *E* region and the FTI Pedersen conductivity in the *F* region, respectively. $W_{\varphi PF}$ and W_{LPF} represent the Pedersen conductivity weighted large-scale winds $W_{\varphi F}$ and W_{LF} along φ and L coordinates in the *F* region. For the present study, following simplifications in the above equations have been made: The ion drift currents are small compared to the total currents in the *F* region and therefore, they have been dropped from equation (2). In the FTI paradigm, the contribution of currents along the geomagnetic field lines to the current continuity equation is small and hence they have not been considered. The Hall conductivity in the *F* region is not considered as it is neg-

ligible compared to the Hall conductivity in the *E* region. During the postsunset period, the winds in *F* region are much larger than those in the *E* region [*Hedin et al.*, 1991, 1996]. Moreover, during this period as the conductivity of the *E* region is greatly reduced because of molecular recombination, the contribution of the *E* region winds to J_φ and J_L would be much smaller than that due the *F* region winds, and hence the *E* region winds have been neglected. As the model meridional and vertical winds required for this study are not available, the term $-B\,\Sigma_{PF}\,W_{LPF}$ has been dropped from equation (2). It should be noted that the circulatory current systems that vary with magnetic declination D (such as presented by *Maeda et al.* [1982] on the basis of MAGSAT data) do not contribute to the FTI currents that are discussed in this paper, as for these currents the resultant values of the FTI currents perpendicular to B in the meridional plane is zero. For the phenomenon under study, the latitudinal and longitudinal extent of the current stream (described by ABCDE) is much larger than its vertical extent. Therefore, for the sake of convenience, the coordinates φ and L have been replaced by Cartesian coordinates x and z. Here E_z represents electric field perpendicular to B in the meridional plane. With the above assumptions, equations (2) and (3) reduce to:

$$J_x = \Sigma_{PT}E_x + \Sigma_{HE}E_z \tag{4}$$

$$J_z = \Sigma_{PT}E_z - \Sigma_{HE}E_x + B\Sigma_{PF}W_{xPF} \tag{5}$$

where

$$\Sigma_{PT} = \Sigma_{PF} + \Sigma_{PE} \tag{6}$$

Here Σ_{PT} is the FTI Pedersen conductivity. Let the distance along a given current flow path be S, where S is measured from 1700 LT (from say the point A as shown in Figure 1). The currents that flow from the presunset side into the postsunset pre-Z_{EFRR-1} region consist of (1) the current in the integrated *F* region denoted by $\check{C}_F$ and (2) the current in the EEJ region denoted by $\check{C}_{EEJ}$. Even though the EEJ and the base of the integrated *F* region are intervened by a region of conductivity much lower than either of these regions, we assume that the EEJ and LSFTI *F* region are electrically well connected. To meet the CCR of the *F* region dynamo, the EEJ current $\check{C}_{EEJ}$ that flows from the presunset side into the postsunset region gets gradually transferred to the LSFTI *F* region and adds to the ambient current $\check{C}_F$. The combination of $\check{C}_F$ and $\check{C}_{EEJ}$ denoted by $\check{C}_{comb}$ then turns upward/poleward and thereafter flows westward for some distance and subsequently joins the daytime Sq current system. This upward/poleward flowing current along with the current from the following morning side meets the CCR of the *F* region dynamo. In addition to $\check{C}_F$ and $\check{C}_{EEJ}$ there is a third current, as pointed out earlier, which is the Hall current that flows across Z_{EFRR-1} along the *x* axis in the *E* region. The density of this Hall current is denoted by J^R_{xH}, where the superscript R denotes the values in the Z_{EFRR-1}.

[16] The current in the LSFTI *F* region and in the upper side of the Flux Tube Integrated (USFTI) *F* region can be divided into a number of current streams of equal widths in each of these regions. Each of these current streams in the LSFTI *F* region will have a corresponding current stream in the EEJ. Let the width of a given current stream at a distance S in the *F* region be δL_F and let the current in it be $\delta\check{C}_F$. Let the total Cowling conductivity of the corresponding current stream in the EEJ at a distance corresponding to S be δ_{EEJ}. The combined current $\delta\check{C}_{comb}$ corresponding to a given current stream in the *F* region at S is given by

$$\delta\check{C}_{comb} = \delta\check{C}_F + \delta\check{C}_{EEJ} = \delta\check{C}_F + \delta\text{€}_{EEJ}\,E_x \tag{7}$$

$\delta\check{C}_{EEJ}$ is given by $\delta_{EEJ}\,E_x$. Here we represent corresponding values of various parameters at A with a superscript 0 except that of $\delta\check{C}_{comb}$. From the current continuity requirement $\delta\check{C}_{comb}$ is assumed to remain constant over a current stream. If $\delta\text{€}^0_{EEJ}$ is υ' times the total conductivity of the corresponding current stream in the *F* region, then

$$\delta\text{€}^0_{EEJ} = \upsilon'\delta L^0_F\Sigma^0_{PT} \tag{8}$$

Even though the value of υ' could not be determined, υ' was varied from 0 to 6 to understand the effect of increase in the conductivity of EEJ on the strength of the EPRE. The conductivity of the EEJ is proportional to the Pedersen conductivity of the *E* region and hence would have a finite value and, therefore, $\upsilon' = 0$ is not realistic and only represents an extreme limit. If during the postsunset period the Cowling conductivity δ_{EEJ} of the corresponding current stream in the EEJ over "x" remains proportional to the FTI Pedersen conductivity of the *E* region and if the extent (size) of the EEJ region remains constant during this period, then, $\delta\text{€}_{EEJ}$ is given by:

$$\delta\text{€}_{EEJ} = \delta\text{€}^0_{EEJ}\left(\Sigma_{PE}/\Sigma^0_{PE}\right) \tag{9}$$

The effective conductivity of the EEJ may be modified by the neutral winds [*Hysell et al.*, 2002]. If known, these modifications can be incorporated into equation (9).

[17] From (8) and (9) we have

$$\delta\text{€}_{EEJ} = \upsilon'\delta L^0_F\Sigma^0_{PT}\left(\Sigma_{PE}/\Sigma^0_{PE}\right) \tag{10}$$

From equation (7) the current density $J^F_S = \delta\check{C}_F/\delta L_F$ is given by:

$$\begin{aligned} J^F_S &= \delta\check{C}_F/\delta L_F = \left(\delta\check{C}_{comb}/\delta L_F\right) - E_x\delta\text{€}_{EEJ}\,/\delta L_F \\ &= \left(\delta\check{C}_{comb}/\delta L_F\right) - \Gamma E_x \end{aligned} \tag{11}$$

where

$$\Gamma = \delta\text{€}_{EEJ}\,/\delta L_F \tag{12}$$

From (10) and (12) we have

$$\Gamma = \upsilon'\Sigma^0_{PT}\left(\Sigma_{PE}/\Sigma^0_{PE}\right)\delta L^0_F/\delta L_F \tag{13}$$

The total current density in the x direction, J_x, consists of the sum of the current component of J^F_S in x direction and the Hall current J^R_{xH}. Therefore, from equations (4) and (11), the total current density J^F_x in the x direction is given by:

$$\begin{aligned} J^F_x &= J^F_S\cos\eta + J^R_{xH} = \left\{\left(\delta\check{C}_{comb}/\delta L_f\right) - \Gamma E_x\right\}\cos\eta + J^R_{xH} \\ &= \Sigma_{PT}E_x + \Sigma_{HE}E_z \end{aligned} \tag{14}$$

Here η is the inclination of the current path from the zonal direction. From equations (5) and (11), the total current J_z^F in the z direction is given by:

$$J_z^F = J_S^F \sin\eta = \left\{\left(\delta\check{C}_{comb}/\delta L_F\right) - \Gamma E_x\right\}\sin\eta = \Sigma_{PT}E_z - \Sigma_{HE}E_x + B\Sigma_{PF}W_{xPF} \quad (15)$$

Solving equations (14) and (15) for E_x and E_z, we have;

$$\gamma_n^2 E_x = \left(\delta\check{C}_{comb}/\delta L_F\right)\left(\Sigma_{PT}\cos\eta - \Sigma_{HE}\sin\eta\right) + B\Sigma_{HE}\Sigma_{PF}W_{xPF} + \Sigma_{PT}J_{xH}^R \quad (16)$$

$$\gamma_n^2 E_z = \left(\delta\check{C}_{comb}/\delta L_F\right)\left(\Sigma_{HE}\cos\eta + \Sigma_{PT}\sin\eta\right) - B\zeta\Sigma_{PF}W_{xPF} + \xi J_{xH}^R \quad (17)$$

Here,

$$\xi = (\Sigma_{HE} - \Gamma\sin\eta), \zeta = (\Sigma_{PT} + \Gamma\cos\eta), \quad (18)$$

$$\gamma_n^2 = \Sigma_{PT}\zeta + \Sigma_{HE}\xi = \Sigma_{PT}^2 + \Sigma_{HE}^2 + \Gamma(\Sigma_{PT}\cos\eta - \Sigma_{HE}\sin\eta) \quad (19)$$

From equations (16) and (17), the electric field E_S along a given current path S is given by ($E_x \cos\eta + E_z \sin\eta$), which yields:

$$\gamma_n^2 E_S = \left(\delta\check{C}_{comb}/\delta L_F\right)\Sigma_{PT} + B\Sigma_{HE}\Sigma_{PF}W_{xPF}\cos\eta - B\zeta\Sigma_{PF}W_{xPF}\sin\eta + (\Sigma_{PT}\cos\eta + \xi\sin\eta)J_{xH}^R \quad (20)$$

Over a given current stream, while the current $\delta\check{C}_{comb}$ remains constant, its width δL_F may vary. Sometime before the Z_{EFRR-1} the current stream makes an upward turn and its width increases by a fairly large factor and hence in that region the term $\delta\check{C}_{comb}/\delta L_F$ is significantly reduced. Moreover near the Z_{EFRR-1}, the EEJ hardly feeds any current to the LSFTI *F* region and therefore, close to the Z_{EFRR-1} region, ($\delta\check{C}_{comb}/\delta L_F$) would be small. In the Z_{EFRR-1} region $E_x = 0$ and, therefore, from (16) the Hall current J_{xH}^R is given by:

$$J_{xH}^R = -B\left(\Sigma_{HE}^R\Sigma_{PF}^R/\Sigma_{PT}^R\right)W_{xPF}^R \quad (21)$$

Here, the superscript R denotes the values of various parameters at Z_{EFRR-1}. We refer the term B ($\Sigma_{HE}\ \Sigma_{PF}/\Sigma_{PT}$) W_{xPF} at a given point as Hall term and denote it with H_T. From the relation (21), the current J_{xH}^R then equals $-H_T^R$. Equation (16) can then be written as,

$$\gamma_n^2 E_x = \left(\delta\check{C}_{comb}/\delta L_F\right)\left(\Sigma_{PT}\cos\eta - \Sigma_{HE}\sin\eta\right) + \Sigma_{PT}\left[H_T - H_T^R\right] \quad (22)$$

Denoting $[H_T - H_T^R]$ with ΔH_T, from (22) we have,

$$E_x = \left(\delta\check{C}_{comb}/\delta L_F\right)\left(\Sigma_{PT}\cos\eta - \Sigma_{HE}\sin\eta\right)\gamma_n^{-2} + \Delta H_T\Sigma_{PT}\gamma_n^{-2} \quad (23)$$

In the LSFTI *F* region, the first term on the RHS of (23) gives the zonal electric field due to Pedersen current denoted by E_{xJ} and the second term gives the zonal electric field due to Hall term denoted by E_{xH}. Thus,

$$E_{xJ} = \left(\delta\check{C}_{comb}/\delta L_F\right)\left(\Sigma_{PT}\cos\eta - \Sigma_{HE}\sin\eta\right)\gamma_n^{-2} \quad (24)$$

$$E_{xH} = \Delta H_T\Sigma_{PT}\gamma_n^{-2} \quad (25)$$

4. Validation of the Proposed Model

[18] The exact determination of currents and electric fields requires detailed two-dimensional solution to the current equations and such a study could not be carried out here. Instead, a simpler approach was adopted. We believe that, although qualitative, this approach provides a good insight into the details of the proposed mechanism. The forms of equations (4) and (5) used in this study are such that one needs to know only the normalized values of the conductivities for the estimation of electric fields. The nighttime value of the Pedersen conductivity in the *E* region, around 1900 LT [*Haerendel and Eccles*, 1992], is the smallest of all the conductivities used in this study. Assuming this conductivity to be the same everywhere in the region of interest, we have used it for normalizing all the conductivities in the *E* and *F* regions. This makes the nighttime equilibrium value of Pedersen conductivity in the *E* region $\Sigma_{PE}^N = 1$ (superscript N represents the nighttime values).

4.1. Determination of Current Density Over a Given Current Path

[19] We now determine the current density over a given current path. In this study the role of currents from the following morning side is not considered in the determination of currents that originate from the presunset side. Using equation (20), the potential drop V_{AE} over a given current path ABCDE, as shown in Figure 1, is given by:

$$V_{AE} = \int E_S dS = \int\left(\delta\check{C}_{comb}/\delta L_F\right)\Sigma_{PT}\gamma_n^{-2}dS + B\int\Sigma_{HE}\Sigma_{PF}\gamma_n^{-2}W_{xPF}dx + \int\Sigma_{PT}\gamma_n^{-2}J_{xH}^R dx - B\int\zeta\Sigma_{PF}\gamma_n^{-2}W_{xPF}\sin\check{I}dz + \int\xi\gamma_n^{-2}J_{xH}^R\sin\check{I}dz \quad (26)$$

where $\check{I}$ is dip angle of the geomagnetic field line at a given location, dx = dS cos η and dz = dS sin η. Here, x, z, and S are in kilometers. In a given meridional plane, when the currents flow from one geomagnetic field line to another, they follow the shortest path. The shortest current path ΔS_{CP} between the two geomagnetic field lines separated by dz is given by sin $\check{I}$ dz.

[20] From the current continuity equation, $\delta\check{C}_{comb}$ in a current stream must remain constant. The first term on the RHS of (26) can be written as $\int(\delta\check{C}_{comb}/\delta L_F^0)\ \text{Б}^{-1}\ \Sigma_{PT}\ \gamma_n^{-2}$ dS, where Б equals ($\delta L_F/\delta L_F^0$). With this modification in (26)

and rearranging the terms in this equation, the expression for $(\delta\check{C}_{comb}/\delta L_F^0)$ can be written as:

$$\left(\delta\check{C}_{comb}/\delta L_F^0\right) = \left[V_{AE} - B\int \Sigma_{HE}\Sigma_{PF}\gamma_n^{-2}W_{xPF}dx - \int \Sigma_{PT}\gamma_n^{-2}J_{xH}^R dx + B\int \zeta\Sigma_{PF}\gamma_n^{-2}W_{xPF}\sin\check{I}dz - \int \xi\gamma_n^{-2}J_{xH}^R \sin\check{I}dz\right] \div \left[\int \Sigma_{PT}\gamma_n^{-2}Б^{-1}dS\right] \quad (27)$$

Equation (27) can be used to determine the current density $(\delta\check{C}_{comb}/\delta L_F^0)$ corresponding to region A if the following parameters are known: (1) the current path, (2) width of the current path, (3) neutral winds in the *F* region, (4) flux tube integrated conductivities, and (5) potential difference V_{AE} between A and E. During evening hours the Sq currents flow poleward and hence V_{AE} would be positive corresponding to upward (poleward) current flow. As V_{AE} is not known, it has been assumed to be zero. Such an assumption would result in an underestimation of $\delta\check{C}_{comb}$. The current density at a distance S over a given current path can be determined using the expression $(Б^{-1}\ \delta\check{C}_{comb}/\delta L_F^0)$ where $Б^{-1}$ corresponds to a given region.

4.2. Probable Current Path

[21] As mentioned in section 2, the value of the current from the following morning side is an essential parameter for the determination of the reversal time of the zonal electric field. However, because of lack of information on the magnitude of the current from the following morning side, the reversal time of the Z_{EFRR-1} was assumed to be 2000 LT on the basis of the VHF radar studies over Jicamarca. Studies of vertical drifts over Jicamarca [*McClure and Peterson*, 1972; *Pingree and Fejer*, 1987] show that during the low solar flux periods, the E_x reversal region Z_{EFRR-2} occurs between 600 and 700 km altitude, while during high solar flux periods, it occurs around 1000 km (B. G. Fejer, private communication, 2008). These studies also show that during late evening hours the zonal electric field (E_x) maximizes at around 1900 LT and remains eastward in the LSFTI *F* region possibly up to Z_{EFRR-1}. On the basis of those observations, it has been assumed in our study that after 1700 LT, a part of the daytime Sq current flows along the current path ABCDE (Figure 1) and then rejoins the daytime Sq current system. Here AB is eastward along x, BCD is along a semielliptic path, and DE is westward along x. We believe that some of the factors that lead to the penetration of the currents into the postsunset region are as follows: Factor 1 is the eastward neutral winds in the *F* region increasing with x give rise to an increasing downward electric field with x. This would lead to the development of an eastward electric field. Factor 2 is the eastward neutral winds in the *F* region increasing with local time giving rise to an increasing current continuity requirement and thus helping in the deeper penetration of currents. Factor 3 is that as the intervening region between the EEJ and base of the *F* region is of conductivity lower than either of the two regions therefore the EEJ current would flow into the base of the *F* region right up to the zonal electric field reversal region Z_{EFRR-1}.

[22] As mentioned earlier, when the currents flow from one field line to another, they would take the shortest current path $(S_{CP})_z$. At a given altitude and in a meridional plane, the $(S_{CP})_z$ between a point (x, 0) and a point (x, z) is given by:

$$(S_{CP})_z = \int_0^z \sin\check{I}dz \quad (28)$$

Here $(S_{CP})_z$, x and z are in kilometers. Let x_T represent the longitudinal distance at which a given current path starts turning upward/poleward, and, x_M the longitudinal distance by which all the currents from presunset side would turn upward/poleward. Four current paths similar to the one shown by ABCDE were used in this study and these are denoted by different values of g. In this study $x_M = 4950$ km which corresponds to 3 h from 1700 LT to 2000 LT. $x_T = 825 \times (g + 1)$, where g varies from 1 to 4 corresponding to the time when the current stream (ABCDE) in the base of the *F* region starts turning upward in the four assumed current paths in succession at 1800 LT, 1830 LT, 1900 LT, and 1930 LT. z_0 and z_R represent lower and upper ends of the current path. The values of x and z along the current paths 1 to 4 are guided by the following constraints:

[23] 1. Along current path AB, $\eta = 0$, $z = z_0$, and x acquires increasing values from 0 to x_T.

[24] 2. Along current path BCD, $x = x_T + (x_M - x_T)\sin\theta$, and $z = z_0 + (z_R - z_0)(1 - \cos\theta)/2$, where θ is in the horizontal plane and is varied from 0 to π to determine the values of coordinates x and z of all the points on a given elliptic path. η is in the vertical plane and is varied from 0 to π.

[25] 3. Along current path DE, $z = z_R$, and x acquires decreasing values from x_T to 0. Here $\eta = \pi$.

[26] The value $(x_M - x_T)$ represents the semimajor axis and $(z_R - z_0)$ represents the minor axis of the elliptic current path. z_R and z_0 represent the distances of the upper and the lower end of the current path, corresponding to the latitudes λ_R and λ_0 respectively, λ_0 being at the dip equator. Here we consider a current path whose lower end is at base of the *F* region at the geomagnetic equator. The geomagnetic latitudes used in this study are given with reference to 200 km altitude for case 1 and 350 km altitude for case 2.

[27] As mentioned in section 3, the width of the current stream δL_F would vary along a current path and it can be represented as a function of S or η. As pointed out earlier, an increase or decrease in the width of the current stream would result in a reduction/increase in the current density. Such a variation in the current density is taken into account through the factor Б in (27). Here, the expression for Б has been derived through geometrical considerations and is not exact. Further, Б1 and Б2 denote the values of Б in the LSFTI *F* region and in the USFTI *F* region respectively. Also, δL_F^1 and δL_F^2 denote the values of δL_F in the LSFTI *F* region and in the USFTI *F* region, respectively.

[28] Let the thickness of the LSFTI *F* region be IJ and that of the USFTI *F* region be JM (Figure 1). Here IJ is the $(S_{CP})_z$ between the latitudes of I and J and JM is the $(S_{CP})_z$ between latitudes of J and M. The currents cover a longitudinal distance corresponding to 3 h local time (1700 LT to 2000 LT) which has been denoted with JC. We assume that if the number of current streams in each of these regions is n, then

the width of the current stream δL_F in the LSFTI F region denoted by δL_F^1 can be represented by:

$$\delta L_F^1 = (IJ \cos\eta + JC \sin\eta)/n \quad (29)$$

Similarly the width of the current stream δL_F in the USFTI F region denoted by δL_F^2 can be represented by:

$$\delta L_F^2 = (JM \cos\eta + JC \sin\eta)/n \quad (30)$$

At A the current flow is assumed to be eastward i.e., $\eta = 0$ therefore from (29) the δL_F^0 at A would be given by IJ/n. The ratio $\delta L_F^1/\delta L_F^0$ denoted here by Б1 is given by:

$$Б1 = \delta L_F^1/\delta L_F^0 = (\rho_1 \cos\eta + \rho_3 \sin\eta) \quad (31)$$

where ρ_1 = IJ/IJ = 1 and ρ_3 = JC/IJ. Similarly $\delta L_F^2/\delta L_F^0$ denoted here by Б2 is given by

$$Б2 = \delta L_F^2/\delta L_F^0 = (\rho_2 \cos\eta + \rho_3 \sin\eta) \quad (32)$$

where ρ_2 = JM/IJ and ρ_3 is same as above.

[29] In the calculations of currents and electric fields, two types of the current widths were used. In case k = 1, the width over the current path was kept constant. In case k = 2, the width over the current path was varied according to (29) and (30) In case k = 1 we assume Б1 = Б2 = 1 all along the current paths while in case k = 2 we use values of Б1and Б2 from (31) and (32).

[30] We now carry out the estimation of ρ_2 for the high solar flux period. During this period the Z_{EFRR-2} (at J) is at around 1000 km altitude (B. G. Fejer, private communication, 2008) while the base of the F region (at I) is at around 350 km [*Anderson et al.*, 1987]. It may be noted that the $(S_{CP})_z$ between two stations with low field line apogee is nearly the same as the difference between the two field line apogees. Therefore, IJ is 650 km. The values of $(S_{CP})_z$ (or IM) between the magnetic equator (λ_0) and the magnetic latitudes (λ_R) of 30°, 40°, and 50° at M are respectively 1583 km, 2537 km, and 3585 km. Therefore, JM for these λ_R values would be 933 km, 1887 km, and 2935 km, respectively. From (31) the values of ρ_2 would therefore be (933/650) = 1.43, (1887/650) = 2.90 and (2935/650) = 4.51, respectively for λ_R of 30°, 40°, and 50° magnetic latitudes.

[31] Next, we estimate ρ_2 for the low solar flux period. During this period Z_{EFRR-2} (at J) is observed at around 650 km altitude [*Fejer et al.*, 1991] while the base of the F region (at I) is around 200 km [*Anderson et al.*, 1987] and, therefore, IJ is 450 km. The values of $(S_{CP})_z$ (or IM) between the magnetic equator (λ_0) and the magnetic latitudes (λ_R) of 30°, 40°, and 50° at M are respectively 1583 km, 2537 km, and 3585 km. As IJ is 450 km, therefore, JM would be 1133 km, 2087 km and 3135 km. Thus ρ_2 for low solar flux period would be (1133/450) = 2.52, (2087/450) = 4.64, and (3135/450) = 6.96 respectively, corresponding to λ_R values of 30°, 40° and 50° magnetic latitude. The current flows upward between 1700 LT to 2000 LT that correspond to a distance of 4950 km. Thus, during low solar flux period, ρ_3 would be (4950/450) = 11.0, while during the period of high solar flux it would be (4950/650) = 7.6.

4.3. Parameters Used in the Numerical Calculations

[32] The following parameters were used in the numerical simulations for estimating the values of zonal eastward electric fields and the vertical drifts for case 1 (low solar flux) and case 2 (high solar flux).

[33] 1. From *Hedin et al.* [1991], zonal neutral winds in the F region are approximated to: $W_{xF} = 140 \sin \pi$ (x/11550) m s^{-1}. For magnetic latitudes greater than 30°, W_{xF} has been assumed to be zero. As the conductivities over the geomagnetic field lines are not known, W_{xPF} could not be determined and has been assumed to be equal to W_{xF}. This would lead to an overestimation of the zonal electric field.

[34] 2. Two different models (LG-1) and LG-2) of the normalized values of Σ_{PE} in the E region have been used in this study to investigate the effect of the value of LGIPC in the E region on the EPRE during low and high solar flux periods. We assume that for LG-1, Σ_{PE} follows the model values of Cowling conductivity in the E region for late evening hours [*Haerendel and Eccles*, 1992] and it can be represented with $\Sigma_{PE}(x) = 10 \exp(-2.302\ x/3300)$ for $x \leq 3300$ km, and $\Sigma_{PE} = 1$ for $x > 3300$ km. The desired value of LGIPC in LG-2 is twice the value for LG-1and, therefore, $\Sigma_{PE}(x)$ in this case can be represented by: $\Sigma_{PE}(x) = 20 \exp(-2.996\ x/3300)$ for $x \leq 3300$ km, and $\Sigma_{PE} = 1$ for $x > 3300$ km. This model represents the variation of Σ_{PE} when the ratio of electron density from day to night is increased by a factor of two. As pointed earlier, the ratio of electron density from day to night increases by a factor of two from the period of low solar flux to the period of high solar flux [*Johnson*, 1961]. Therefore, LG-1 and LG-2 are used respectively for case 1 and case 2.

[35] 3. $\Sigma_{HE}/\Sigma_{PE} = 1.7$ during 1700 LT to 2000 LT in the region of interest [*Heelis et al.*, 1974].

[36] 4. To cover a large range of currents in the EEJ, the factor υ' (a factor proportional to the ratio of the total Cowling conductivity of the EEJ to that of the conductivity of the LSFTI F region as given by the expression (10), was varied from 0 to 6.

[37] 5. To study the role of key factor 3 in accounting for the variation in the EPRE under differing solar conditions, we used the normalized value of Σ_{PF} as a function of altitude at 2100 LT under solar minimum and maximum conditions from *Anderson et al.* [1987, Figure 9]. These normalized FTIC values are dimensionless and are denoted here by $\Sigma_{AM}(z)$ and are given up to 22° for the low solar flux period and 25° for the high solar flux period. From Anderson's results [*Anderson et al.*, 1987, Figure 9] the ratio of the average normalized value of Σ_{PF} for the high solar flux period to the low solar flux period turns out to be nearly four and, therefore, we maintain this ratio in the extrapolated value of Σ_{PF} as well. We assume that the FTIC at 2100 LT decrease exponentially beyond these latitudes such that the FTIC values at the geomagnetic latitude of 50° are 0.4 and 1.6 for cases 1 and 2, respectively.

[38] For this study we require values Σ_{AM} both as a function of x and z, both for cases 1 and 2 for the period from 1700 LT to 2000 LT. We should note in this connection that Σ_{PT} variation with "x" from (1700 to 2000 LT) can change significantly with "z." However, these values are available only as a function of z and that too at 2100 LT. We carried out the studies for two different scenarios: one in which the $\Sigma_{AM}(z)$ does not vary with x (denoted as extrapolation 1)

and the other in which $\Sigma_{AM}(z)$ decreases with x at the same rate as the chemical loss of ions at 300 km (denoted as extrapolation 2). Mathematically, the expression Σ_{PT} (x, z) used for extrapolation is:

$$\Sigma_{PT}(x, z) = \Sigma_{AM}(z) \exp[\sigma \times (6600 - x)] \quad (33)$$

In "extrapolation 1" Σ_{PF} varies only with z and not with x and so $\sigma = 0$. In "extrapolation 2" Σ_{PF} decreases along x at the same rate as the chemical loss of ions at 300 km which is 10^{-4} s^{-1} [*Shimazaki*, 1964] and hence $\sigma = 2.18 \times 10^{-4}$. We have estimated V_p using both these types of extrapolations for a few cases and we find that the values were not significantly different. Some of the values of EPRE from the two extrapolations are given in section 4.4 for comparison. However, to avoid any ambiguity in the estimates that might arise because of cumulative uncertainties by assuming the extrapolation 2, we have carried out simulations using extrapolation 1. Although not exact, we believe that through the use of extrapolation 1 any unknown error is not introduced in the results.

4.4. Results

[39] The vertical drift velocity V_{yH} due the Hall term ΔH_T was estimated from (25) for both cases 1 and 2. For case 1, it was found to be 0.9, 1.1, and −3.4 m s^{-1}, respectively at 1800, 1830, and 1900 LT while for case 2, it was found to be −2.1, −2.0, and −4.1 m s^{-1} for the same times. These vertical drift velocities are much smaller than the vertical drift velocities from the current term (24) given in Figures 3, 4, and 5 described below. Therefore, for simplicity, the Hall term is neglected in the present study for the estimation of the vertical drift velocity V_y.

[40] Using equations (27) and (24), the values of current $(\delta C_{comb}/\delta L_F^0)$ and E_x/B was estimated using extrapolation 1 for cases 1 and 2 for four different current paths g = 1 to 4, four different values of $\upsilon' = 0$, 2, 4 and 6, and for three current return latitudes $\lambda_R = 30°$, 40° and 50°. An increase in υ' leads to an increase in $\delta\check{C}_{comb}$ through (10) and (7). An increase in υ' also leads to an increase in Γ through (13) thereby an increase in γ_n^2 through (19). As $\delta\check{C}_{comb}$ and γ_n^2 increase with υ' it is difficult to determine analytically from (24) how E_x would vary with the increase of υ'. An increase of υ' gives rise to an increase of the conductivity of the EEJ in relation to that in the *F* region through (8). Therefore, realistically υ' would have values in a limited range. As pointed out earlier $\upsilon' = 0$ is not realistic and has been used only as an extreme limit. The ratio of conductivity of the *E* region from presunset to the postsunset period is not dependent on υ' and hence it does not affect the LGIPC used in this study. The LG-1 (section 4.3) was used in case 1 and LG-2 (section 4.3) in case 2. Calculations were carried out for two different "types" of current streams: (1) with constant width represented by k = 1 and (2) with width varying as appropriate to the region represented by k = 2. Б1 and Б2 required for the estimation of $(\delta C_{comb}/\delta L_F^0)$ are given by (31) and (32) and the values of ρ_1, ρ_2, and ρ_3 for both cases 1 and 2 are given in section 4.2. Some of the important results obtained from these studies are shown in Figures 2–5.

[41] The variation in the strength of the current density $(\delta C_{comb}/\delta L_F^0)$ is shown in Figure 2 for current path along S: (1) with constant width (k = 1) and (2) with varying width (k = 2) for both case 1 and case 2. As expected, $\delta C_{comb}/\delta L_F^0$ increases monotonically with an increase in λ_R for both the cases. Further, its magnitude is larger for case 2 as compared to case 1. From Figure 2 it can also be seen that $C_{comb}/\delta L_F^0$ is larger for k = 2 as compared to that for k = 1. As the path represented by k = 2 is more realistic than that corresponding to k = 1, in this study all the detailed calculations on the vertical drift velocities have been made using k = 2.

[42] The vertical drift velocities $V_y = E_x/B$ for cases 1 and 2 as a function of local time are shown in Figures 3 and 4. In both the cases, an increase of V_y with local time before x_T is due to a decrease in conductivity along the current path, while the decrease after x_T is due to the currents turning upward. In case 1, V_y maximizes for path 3 while in case 2 it maximizes for path 2. In both the cases they maximize close to 1900 LT. Both in case 1 and case 2, for g = 4 there is no increase in V_y between the period 1900 to 1930 LT as there is no decrease in conductivity during this period.

[43] The peak values of V_y denoted here by V_p for case 1 are 22.0 m s^{-1}, 33.5 m s^{-1} and 35.7 m s^{-1} respectively, for λ_R = 30°, 40° and 50°. For case 2 these are 44.6 m s^{-1}, 76.3 m s^{-1}, and 77.9 m s^{-1} (not shown in Figures 3 and 4). Thus, V_p values for case 2 are more than two times larger as compared to those for case 1. The ratios of V_p between case 2 and case 1 agree qualitatively with the Jicamarca radar observations [*Fejer et al.*, 1991]. We investigated the dependence of V_p on the chemical loss rate of ions using extrapolation 2 (section 4.3) and found that it does not significantly differ from the value of E_x/B from extrapolation 1 used in this study. For example in case 2 for $\upsilon' = 2$, $\lambda_R = 40°$, V_p was 76.3 m s^{-1} for extrapolation 1 and was 74.7 for extrapolation 2. The cause of such a decrease is as follows. While for extrapolation 2, $(\delta C_{comb}/\delta L_F)$ is larger compared to that for extrapolation 1, reverse is true for conductivity at 1900 LT.

[44] A numerical simulation was also carried out for to investigate the effect of the LGIPC in the *E* region on the magnitude of the EPRE. Two values of LGIPC in the *E* region denoted by LG-1 and LG-2 as defined in section 4.3 were used. For case 1, ($\upsilon' = 2$, g = 2, and $\lambda_R = 40°$) the V_p was found to be 33.5 m s^{-1} and 38.5 m s^{-1} respectively, for LG-1 and LG-2. For the same parameters but for case 2, the values of V_p were 64.6 m s^{-1} and 76.3 m s^{-1}. Thus an increase in the LGIPC in the *E* region by a factor of two results in increases of V_p only by 15% in case 1 and 18% in case 2. On the basis of the studies of seasonal variation of V_p, it is generally believed that the LGIPC in the *E* region can greatly affect the V_p amplitude. However, *Batista et al.* [1986] find that the relationship between the sunset duration that affects the LGIPC in the *E* region at sunset time and V_p peak amplitude does not seem to be all that straightforward. Therefore, the confirmation of the present results can best be carried out through a rigorous numerical simulation for a station with specifications similar to the one used here.

[45] From Figure 4 we can see that for case 2 the largest vertical drift velocity V_p corresponds to path 2 (g = 2) when E_x/B maximizes at 1900 LT. Therefore, we use path 2 to study the role of the EEJ in the development of the EPRE. Figure 5 shows that for g = 2 and $\lambda_R = 40°$, V_p decreases with the increase of υ' from 0 to 6. V_p is 88.8 m s^{-1} for $\upsilon' = 0$ while it is 59.1 m s^{-1} for $\upsilon' = 6$ which is a decrease of 33.5%. This slow change in V_p with the increase of υ' arises because of the fact that the terms $(\delta C_{comb}/\delta L_F^0)$ and γ_n^2, which determine E_x from

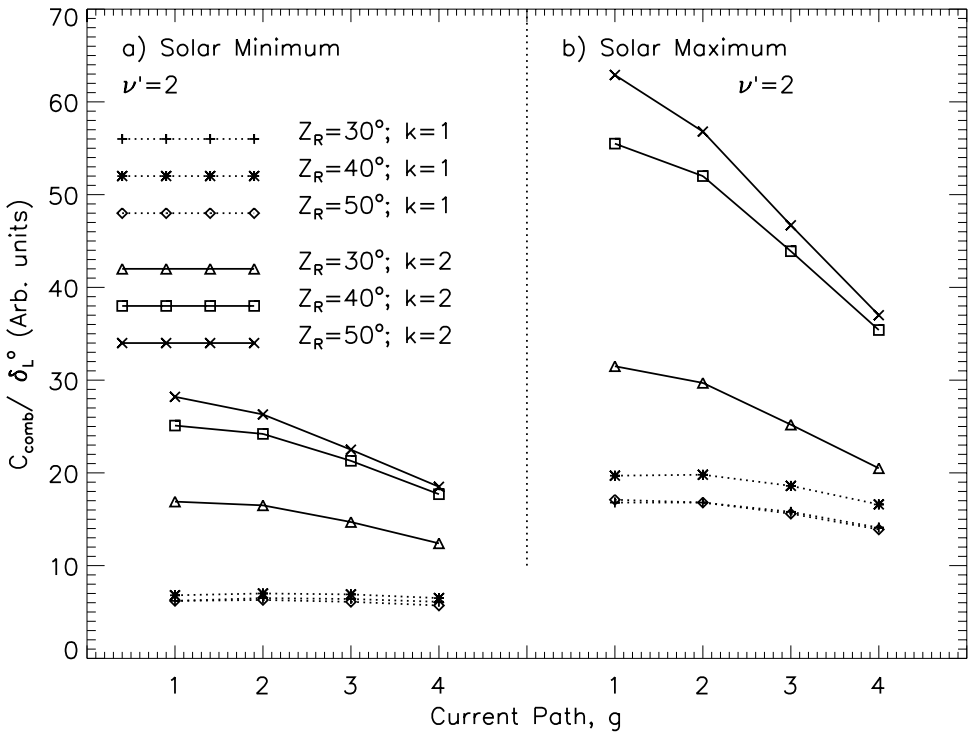

Figure 2. The variation in ($\delta\check{C}_{comb}/\delta L_F^0$) with respect to the different current paths g (1, 2, 3, and 4) for solar minimum (case 1) and solar maximum (case 2) when $\upsilon' = 2$. Plots are shown for three different current path return latitudes ($\lambda_R = 30°$, 40°, and 50°) and two different types of current streams denoted by k = 1 and k = 2. k = 1 represents a current stream with a constant width along the current path while k = 2 represents the current stream with width appropriate to a given region along a given current path. From this figure it can be seen that large λ_R would yield larger current because of increased dynamo action as well as because of increased width of the current path along ABCDE (Figure 1). As the zonal wind W_{xF} has been assumed to be zero beyond $\lambda = 40°$, the increase of ($\delta\check{C}_{comb}/\delta L_F^0$) with the increase in latitude is not very large beyond 40°.

(24), increase with υ'. With the increase of υ', the increase of ($\delta C_{comb}/\delta L_F^0$) can be visualized from (10) and (7) while the increase of γ_n^2 can be visualized from (13) and (19). In (24) while the current appears in the numerator, the conductivity appears in the denominator. From this study, it can be inferred that V_p would not be affected significantly by small variations either in the strength of EEJ or in the FTIC in the LSFTI *F* region at 1700 LT. From this result it should not be inferred that the EEJ plays only a negative role in the development of the EPRE. One of the ways in which the EEJ might be indirectly contributing to the development of the EPRE is through feeding current in the base of the *F* region right up to Z_{EFRR-1} and thus enabling the flow of current in the lower part of the LSFTI *F* region.

5. Discussion and Summary

[46] Typical features TF 1, TF 2, and TF 3 of the eastward electric field associated with the EPRE have been discussed in section 2. According to the current understanding, there are two key factors that are associated with the development of the EPRE. The key factor 1 is the presence of eastward neutral wind in the thermosphere and the key factor 2 is a rapid decrease in the FTIC of the *E* region after the sunset. Beginning with the studies of *Rishbeth* [1971] and *Heelis et al.* [1974] these two factors have been widely used in the literature. Model studies for the EPRE generation that used these factors explicitly are mechanism 1 by *Farley et al.* [1986] that utilized the Hall conductivity gradient in the off equatorial region line-tied to the equatorial *F* region, and mechanism 2 by *Haerendel and Eccles* [1992] that utilized the gradient in Cowling conductivity of the EEJ. *Eccles* [1998] examined the suitability of these two mechanisms for the development of the EPRE by altering the Hall conductivity in his model calculations (1) exclusively outside the EEJ region, and (2) completely within the EEJ region and concluded that [*Eccles*, 1998, p. 26,717] "both regions of mechanism 1 and 2 are involved in the circuit but are only limited modifier of EPE" (which is EPRE in this study). As an alternative to these mechanisms, *Eccles* [1998] proposed that the zonal electric field is a result of curl-free nature of the electric field when the vertical electric field changes rapidly near sunset. While the curl-free nature of the electric field can be used to determine the magnitude of the zonal electric field when the vertical electric field as a function of x and y is known, it should be noted that one still requires a mechanism that leads to the modification of the vertical electric field suitably to give the observed zonal electric field.

[47] The zonal winds in the tropical *F* region give rise to polarization electric fields and the CCR in this region [*Rishbeth*, 1971]. In this study we propose that to meet this current requirement, the daytime Sq currents get diverted

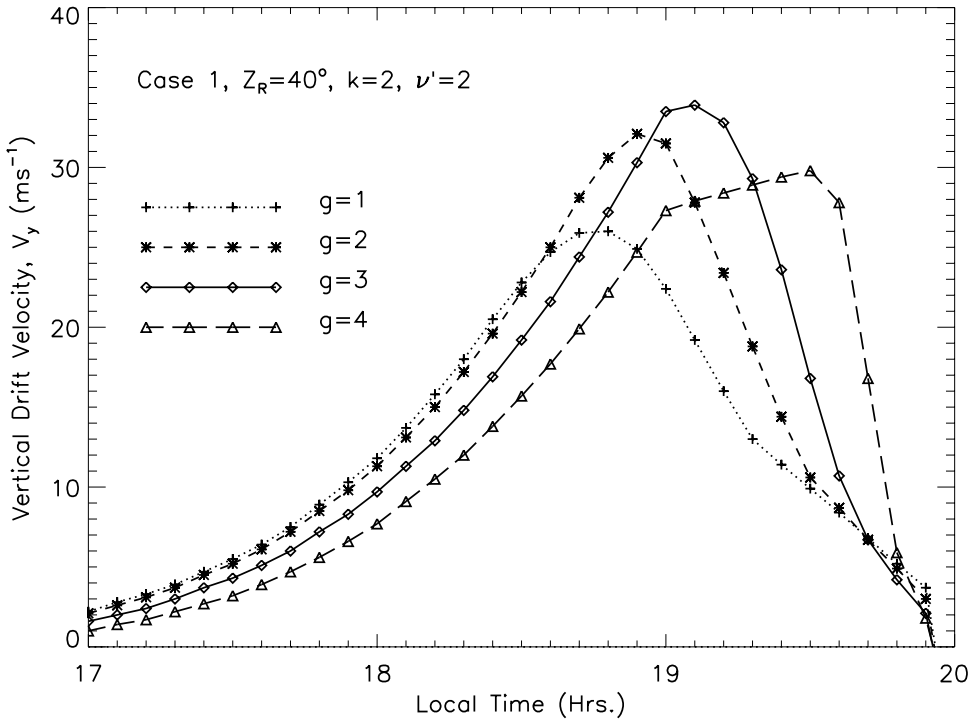

Figure 3. Values of V_y (=E_x/B) are shown for case 1, $\lambda_R = 40°$ latitude, k = 2, LG-1, $\upsilon' = 2$, and g = 1, 2, 3, and 4. V_p (the peak value of V_y) has a maximum value of 26.1 m s^{-1} at 1848 LT, 32.1 m s^{-1} at 1900 LT, 33.5 m s^{-1} at 1900 LT, and 29.5 m s^{-1} at 1900 LT for current paths 1, 2, 3, and 4, respectively. It can be seen that V_p has the largest value for the current path 3 (g = 3), which is not much different from the value for path 2 (g = 2).

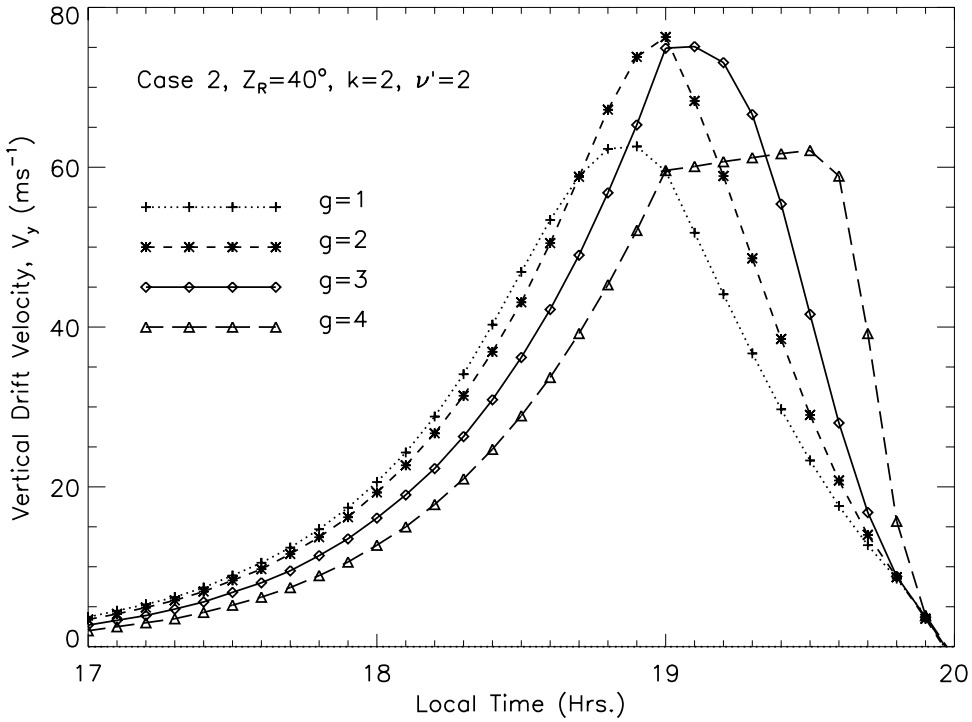

Figure 4. Values of V_y (=E_x/B) are shown for case 2, $\lambda_R = 40°$ latitude, k = 2, LG-2, $\upsilon' = 2$, and g = 1, 2, 3, and 4. V_p (the peak value of V_y) has a maximum value of 62.4 m s^{-1} at 1854 LT, 75.9 m s^{-1} at 1900 LT, 75.3 m s^{-1} at 1900 LT, and 62.2 m s^{-1} at 1900 LT for current paths 1, 2, 3, and 4, respectively. In case 2, V_p has the largest value for the current path 2. It can be noted that the V_p estimated for high solar flux conditions is more than a factor of two larger than for the low solar flux conditions.

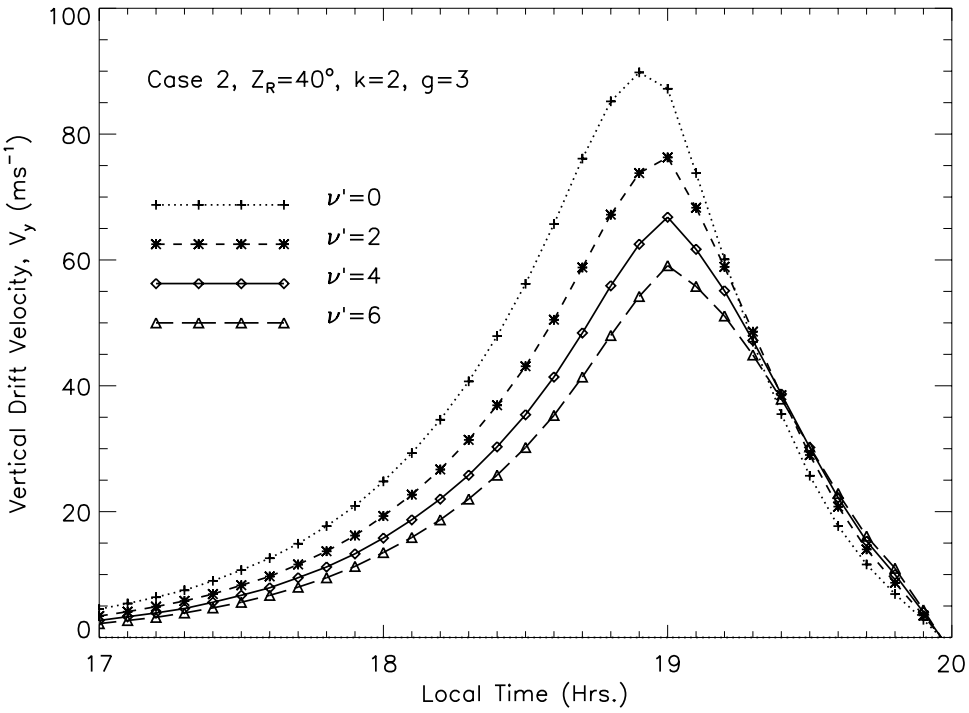

Figure 5. Values of V_y (=E_x/B) are shown for case 2, $\lambda_R = 40°$ latitude, k = 2, g = 2, and $\upsilon' = 0$, 2, 4, and 6. V_p (the peak value of V_y) are 88.8, 76.4, 66.8, and 59.3 m s^{-1} for $\upsilon' = 0$, 2, 4, and 6, respectively. While the maxima for $\upsilon' = 0$ occurs at 1854 LT, the maxima for the other three occur close to 1900 LT. This implies that the current from the EEJ entering the base of the *F* region shifts the time of maxima of E_x to a later time.

(extended) into the postsunset equatorial region. These zonal currents in the equatorial region not only flow in the EEJ, as proposed by *Haerendel and Eccles* [1992], but also in the LSFTI *F* region, as proposed here. These currents then turn poleward to meet the CCR of the *F* region dynamo followed by a westward flow to join the evening time Sq current system. We propose that the current that is responsible for the development of EPRE is an extension of the daytime Sq current system that gets diverted into the postsunset region to meet the current continuity requirement of the postsunset *F* region dynamo. For a given current, the largest electric field will be produced around 1900 LT where the integrated Cowling conductivity of the *E* region stops decreasing further and acquires a nighttime equilibrium value. The decrease in the zonal electric field after acquiring a large value is not only due to the currents turning upward but also due to the increase in the width of the current path.

[48] As proposed in section 2, the typical feature 2 (the reversal of zonal electric field at around 2000 LT) is due to the interplay between the currents from the presunset side and the following morning side. The current from the following morning side is believed to be due to the potential difference between the dawn and dusk terminators that is created by the daytime *E* region dynamo. It is proposed that the current from the presunset side will flow into the postsunset region when the CCR of the *F* region dynamo is larger than what can be met by the currents from the following morning side. The amplitude of the eastward neutral wind in the *F* region increases appreciably with local time till 2030 LT, which results in an increase in the dynamo action until 2030 LT. This enables penetration of currents from the daytime into the postsunset region to meet the CCR of the *F* region dynamo.

[49] From the generalized Ohm's law one can see that the current over a given path is a function of both neutral winds and conductivities and hence, the zonal electric field is dependent only on winds and conductivities in the *E* and *F* regions. As the neutral winds do not vary appreciably over a solar cycle [*Hedin et al.*, 1991], we propose (as pointed out in section 2) that the change in the intensity of the EPRE over a solar cycle (typical feature 3) is due to the change in the FTIC of the ionospheric *F* region during this period. This change in the FTIC with solar flux is referred to as the key factor 3. This change in FTIC from low to high solar flux periods is brought about by the stronger development of the EIA and over all increase in the electron density in the *F* region during high solar flux periods. To illustrate this conjecture, we have used in our numerical simulation the values of normalized FTIC in the *F* region at 2100 LT for the two periods given by *Anderson et al.* [1987, Figure 9]. The details of normalization of the FTIC are given in section 2. The numerical simulation requires FTIC values for the period 1700 LT to 2000 LT but these are available for only 2100 LT from *Anderson et al.* [1987]. Over a given latitude we used the value of FTIC at 2100 LT for the period from 1700 LT to 2000 LT. This has been denoted as extrapolation 1. With the FTIC values at 2100 LT as the reference, we tried another type of extrapolation 2 wherein the conductivity changes with a model rate of chemical loss with local time during 1700 to 2100 LT. As described in sections 4.3 and 4.4, we did not find significant difference in the EPRE magnitudes between the two types of

extrapolations, and so to keep the procedure simple, we used extrapolation 1.

[50] Another factor that can contribute to the increase of the amplitude of EPRE is the LGIPC in the *E* region. From the study of seasonal variation of EPRE, it is generally believed that a small change in LGIPC can result in a large change in the amplitude of EPRE. As pointed out in section 2, *Batista et al.* [1986] find that the relationship between the sunset duration that affects the LGIPC in the *E* region at sunset time and V_p peak amplitude does not seem to be all that straightforward. For example, over Huancayo the amplitudes are greater during summer than during winter months, but the sunset duration in December are greater than in July, showing that there may be other factors, besides the LGIPC in the *E* region, that have influence on the V_p amplitudes. A rigorous numerical simulation for a station when the solar terminator is aligned with the magnetic meridian is required to determine the relative importance of the LGIPC in the *E* region in accounting for the increase of EPRE amplitude with the solar flux. In the present numerical simulation when the LGIPC is increased by a factor of two, it gives an increase in the amplitude of EPRE only by less than 20%.

[51] Using the current system described above and illustrated in Figure 1, values of V_p have been estimated for case 1 and case 2 and are shown in Figures 3 and 4. It can be seen that the V_p for case 2 is not only sufficiently large, but is also more than two times larger than the E_x/B for case 1. This indicates that the variation in the FTIC in the *F* region from low to high solar flux periods, can account for the observed typical feature 3 of the EPRE. An increase in the solar flux not only results in an overall increase in the electron density (thereby FTIC) in the ionospheric *F* region but also in the invigoration of the *F* region fountain effect when the zonal electric fields are eastward thus leading to the development of EIA.

[52] The electrical coupling effect of the FTIC of the EIA on the EPRE is almost instantaneous. Growth time of EIA in the daytime can be a few hours [*Hanson and Moffett*, 1966; *Walker and Strickland*, 1981] and one would expect a similar growth time during late evening hours as well. A numerical simulation of N_{max} by *Klobuchar et al.* [1991] for the postsunset period shows that between 1700 to 2000 LT even a medium EPRE leads to an increase of N_{max} in the tropical *F* region by about a factor of two. As the time duration between 1700 LT and the formation of the peak in the EPRE is comparable to the growth time of EIA, therefore, for EPRE to be strong, it is essential that a fairly strong EIA is present at 1700 LT, which is the time of initiation of the EPRE. In our model the zonal winds turn eastward at 1700 LT. In case this requirement is met then the electric field associated with the EPRE can support EIA during the postsunset period and vice versa and thus the two are mutually sustaining. Thus the presence of a strong EIA near 1700 LT could contribute to the enhancement of the EPRE amplitude through a delayed positive feedback between the EPRE and EIA in the course of the EPRE development from 1700 LT. However, its significance could not be quantified from the present model calculations.

[53] In summary, the conditions necessary for the development of a strong EPRE during the postsunset period are (1) the zonal neutral winds continue to remain eastward after their reversal at around 1700 LT at least up to 2000 LT and (2) the presence of a strong EIA at around 1700 LT when the neutral winds in the *F* region reverse from the westward to the eastward direction. The observed variability in the strength of the EPRE with respect to the variability with the solar flux is due to (1) the variation of the zonal winds in the tropical *F* region, (2) value of electron density in the *F* region due to the variability of solar flux, and (3) variability of EIA at 1700 LT. The present work has added one more key factor KF3 in terms of the increased FTIC of the tropical *F* region. With the addition of this key factor KF3, all the three typical features TF1, TF2, and TF3 can be explained. In addition to bringing to light the possibility of a fundamental factor contributing to the development of the EPRE, this new mechanism clearly offers one of the pathways by which the nighttime equatorial upper atmospheric phenomena are influenced by those that occur during the presunset period. This study thus emphasizes the necessity of investigating the daytime and nighttime ionosphere/thermosphere regions as a coupled system.

[54] **Acknowledgments.** The authors are indebted to P. K. Kaw for his help in carrying out many detailed discussions. We are highly grateful to the referees for taking keen interest in the contents of the paper and making very useful suggestions. This work is supported by Department of Space, Government of India.

[55] Amitava Bhattacharjee thanks the reviewers for their assistance in evaluating this paper.

References

Abdu, M. A., J. A. Bittencourt, and I. S. Batista (1981), Magnetic declination control of the equatorial *F* region dynamo electric field development and spread *F*, *J. Geophys. Res.*, *86*, 11,443–11,446, doi:10.1029/JA086iA13p11443.

Anderson, D. N., R. A. Heelis, and J. P. McClure (1987), Calculated nighttime eastward plasma drift velocities at low latitudes and their solar cycle dependence, *Ann. Geophys.*, *5A*(6), 435–442.

Balsley, B. B. (1973), Electric fields in the equatorial ionosphere: A review of techniques and measurements, *J. Geophys. Res.*, *35*, 1035–1044.

Batista, I. S., M. A. Abdu, and J. A. Bittencourt (1986), Equatorial F region vertical plasma drifts: Seasonal and longitudinal asymmetries in the American sector, *J. Geophys. Res.*, *91*, 12,055–12,064, doi:10.1029/JA091iA11p12055.

Crain, D. J., R. A. Heelis, G. J. Bailey, and A. D. Richmond (1993), Low-latitude plasma drifts from a simulation of the global atmospheric dynamo, *J. Geophys. Res.*, *98*, 6039–6046, doi:10.1029/92JA02196.

Du, J., and R. J. Stening (1999), Simulating the ionospheric dynamo—II. Equatorial electric fields, *J. Atmos. Sol. Terr. Phys.*, *61*, 925–940, doi:10.1016/S1364-6826(99)00042-5.

Eccles, J. V. (1998), Modeling investigation of the evening prereversal enhancement of the zonal electric field in the equatorial ionosphere, *J. Geophys. Res.*, *103*, 26,709–26,720, doi:10.1029/98JA02656.

Farley, D. T. (1959), A theory of electrostatic fields in a horizontally stratified ionosphere subject to a vertical magnetic field, *J. Geophys. Res.*, *64*, 1225–1233, doi:10.1029/JZ064i009p01225.

Farley, D., B. Balsey, R. Woodman, and J. McClure (1970), Equatorial spread *F*: Implications of VHF radar observations, *J. Geophys. Res.*, *75*(34), 7199–7216, doi:10.1029/JA075i034p07199.

Farley, D. T., E. Bonelli, B. G. Fejer, and M. F. Larsen (1986), The prereversal enhancement of the zonal electric field in the equatorial ionosphere, *J. Geophys. Res.*, *91*, 13,723–13,728, doi:10.1029/JA091iA12p13723.

Fejer, B. G. (1981), The equatorial ionospheric electric fields: A review, *J. Atmos. Terr. Phys.*, *43*, 377–386, doi:10.1016/0021-9169(81)90101-X.

Fejer, B. G., D. T. Farley, R. F. Woodman, and C. Calderon (1979), Dependence of the equatorial *F* region vertical drifts on seasons and solar cycle, *J. Geophys. Res.*, *84*, 5792–5796, doi:10.1029/JA084iA10p05792.

Fejer, B. G., E. R. dePaula, S. A. Gonzalez, and R. F. Woodman (1991), Average vertical and zonal *F* region plasma drifts over Jicamarca, *J. Geophys. Res.*, *96*(A8), 13,901–13,906, doi:10.1029/91JA01171.

Fesen, C. G., G. Crowley, R. G. Roble, A. D. Richmond, and B. G. Fejer (2000), Simulation of the pre-reversal enhancement in the low latitude vertical ion drifts, *Geophys. Res. Lett.*, *27*(13), 1851–1854, doi:10.1029/2000GL000061.

Goel, M. K., S. S. Singh, and B. C. N. Rao (1990), Postsunset rise of the *F* layer height in the equatorial region and its relation to the *F* layer dynamo polarization fields, *J. Geophys. Res.*, *95*, 6237–6246, doi:10.1029/JA095iA05p06237.

Haerendel, G., and J. V. Eccles (1992), The role of equatorial electrojet in the evening ionosphere, *J. Geophys. Res.*, *97*, 1181–1197, doi:10.1029/91JA02227.

Hanson, W. B., and D. K. Bamgboye (1984), The measured motion inside equatorial plasma bubbles, *J. Geophys. Res.*, *89*, 8997–9008, doi:10.1029/JA089iA10p08997.

Hanson, W. B., and R. J. Moffett (1966), Ionization transport effect in the equatorial F region, *J. Geophys. Res.*, *71*, 5559–5572.

Hedin, A. E., et al. (1991), Revised global model of thermosphere winds using satellite and ground-based observations, *J. Geophys. Res.*, *96*, 7657–7688, doi:10.1029/91JA00251.

Hedin, A. E., et al. (1996), Empirical wind model for the upper, middle and lower atmosphere, *J. Atmos. Terr. Phys.*, *58*, 1421–1447, doi:10.1016/0021-9169(95)00122-0.

Heelis, R. A., P. C. Kendall, R. J. Moffett, and D. W. Windle (1974), Electrical coupling of the *E*- and *F*-regions and its effect on *F*-region drifts and winds, *Planet. Space Sci.*, *22*, 743–756, doi:10.1016/0032-0633(74)90144-5.

Hysell, D. L., J. L. Chau, and C. G. Fesen (2002), Effects of large horizontal winds on the equatorial electrojet, *J. Geophys. Res.*, *107*(A8), 1214, doi:10.1029/2001JA000217.

Jayachandran, B., N. Balan, S. P. Namboothiri, and P. B. Rao (1987), HF Doppler observations of vertical plasmas drifts in the evening *F* at the equator, *J. Geophys. Res.*, *92*, 11,253–11,256, doi:10.1029/JA092iA10p11253.

Jee, G. R., R. W. Schunk, and L. Scgerkuess (2007), Analysis of TEC data from the TOPEX/Poseidon mission, *J. Geophys. Res.*, *109*, A01301, doi:10.1029/2003JA010058.

Johnson, F. S. (Ed.) (1961), *Satellite Environment Handbook*, Stanford Univ. Press, Stanford, Calif.

Klobuchar, J. A., D. N. Anderson, and P. H. Doherty (1991), Model studies of the latitudinal extent of the equatorial anomaly during equinoctial conditions, *Radio Sci.*, *26*, 1025–1047, doi:10.1029/91RS00799.

Maeda, H., T. Iyemori, T. Araki, and K. Kamei (1982), New evidence of a meridional current system in the equatorial ionosphere, *Geophys. Res. Lett.*, *9*, 337–340, doi:10.1029/GL009i004p00337.

McClure, J. P., and V. L. Peterson (1972), Plasma transport in the equatorial *F* region, *Radio Sci.*, *7*, 539–547, doi:10.1029/RS007i005p00539.

Mendillo, M., J. Meriwether, and M. Biondi (2001), Testing the thermospheric wind suppression mechanism for day-to-day variability of equatorial spread *F*, *J. Geophys. Res.*, *106*, 3655–3664, doi:10.1029/2000JA000148.

Muggleton, L. M. (1975), A method of predicting foE at any time and place, *Telecommun. J.*, *42*, 413–418.

Namboothiri, S. P., B. Jayachandran, N. Balan, and P. B. Rao (1988), Vertical plasma drifts in the post sunset *F* region at the magnetic equator, *J. Atmos. Terr. Phys.*, *50*, 1087, doi:10.1016/0021.

Pallamraju, D., S. Chakrabarti, and C. E. Valladares (2004), Magnetic storm induced enhancement in neutral composition at low-latitudes as inferred by O(^1D) dayglow measurements From Chile, *Ann. Geophys.*, *22*, 3241–3250.

Pingree, J. E., and B. J. Fejer (1987), On the height variation of the equatorial *F* region vertical plasma drift, *J. Geophys. Res.*, *92*, 4763–4766, doi:10.1029/JA092iA05p04763.

Prakash, S., and P. Muralikrishna (1981), *E* and *F* region electric fields over the dip equator, *J. Geophys. Res.*, *86*, 2095–2098, doi:10.1029/JA086iA04p02095.

Raghavarao, R., M. Nageshwararao, J. H. Sastri, G. D. Vyas, and M. Sriramarao (1988), Role of equatorial ionization anomaly in the initiation of equatorial spread *F*, *J. Geophys. Res.*, *93*, 5959–5964, doi:10.1029/JA093iA06p05959.

Rastogi, R. G., S. Alex, and P. V. Korparkar (1989), Equatorial spread *F* and ionospheric electron content at low latitude, *J. Geomagn. Geoelectr.*, *41*, 753–767.

Rishbeth, H. (1971), Polarization fields produced by winds in the equatorial *F*-region, *Planet. Space Sci.*, *19*, 357–369, doi:10.1016/0032-0633(71)90098-5.

Shimazaki, T. (1964), Night time variations of *F*-region electron density profiles at Puerto Rico, *J. Geophys. Res.*, *69*, 2781–2797, doi:10.1029/JZ069i013p02781.

Sridharan, R., D. Pallam Raju, R. Raghavarao, and P.V. S. Ramarao (1994), Precursor to equatorial spread-*F* in OI 630.0 nm dayglow, *Geophys. Res. Lett.*, *21*, 2797–2800, doi:10.1029/94GL02732.

Stening, R. J. (1981), A two-layer ionospheric dynamo calculation, *J. Geophys. Res.*, *86*, 3543–3550, doi:10.1029/JA086iA05p03543.

Takeda, M., and Y. Yamada (1987), Simulation of the ionospheric electric fields and geomagnetic field variations by the ionospheric dynamo for different solar activity, *Ann. Geophys., Ser. A*, *5*, 429–434.

Tsunoda, R. (1985), Control of the seasonal and longitudinal occurrence of equatorial scintillations by the longitudinal gradient in integrated E region Pedersen conductivity, *J. Geophys. Res.*, *90*(A1), 447–456, doi:10.1029/JA090iA01p00447.

Valladares, C., S. Basu, K. Groves, M. P. Hagan, D. Hysell, A. J. Mazzella Jr., and R. E. Sheehan (2001), Measurement of the latitudinal distributions of total electron content during equatorial spread *F* events, *J. Geophys. Res.*, *106*, 29,133–29,152, doi:10.1029/2000JA000426.

Walker, G. O., and A. E. Strickland (1981), A comparison of the ionospheric equatorial anomaly in the east Asian and the American regions at sunspot minimum, *J. Atmos. Terr. Phys.*, *43*(5–6), 589–595, doi:10.1016/0021-9169(81)90121-5.

Woodman, R. F. (1970), Vertical drift velocities and east-west electric fields at the magnetic equator, *J. Geophys. Res.*, *75*, 6249–6259, doi:10.1029/JA075i031p06249.

D. Pallamraju, S. Prakash, and H. S. S. Sinha, Physical Research Laboratory, Ahmedabad 380009, India. (sprakash_prl@yahoo.com)